# Replica-exchange Nosé-Hoover dynamics for Bayesian learning on large datasets

**Rui Luo**\*12, **Qiang Zhang**\*1, **Yaodong Yang**12, and **Jun Wang**12
1University College London, <sup>2</sup>Huawei Technologies

### **Abstract**

In this paper, we propose a new sampler for Bayesian learning that can efficiently draw representative samples from complex posterior distributions with multiple isolated modes in the presence of mini-batch noise. This is done by simulating a collection of replicas in parallel with different temperatures. When evolving the Nosé-Hoover dynamics, the sampler adaptively neutralizes the mini-batch noise. To approximate the detailed balance, configuration exchange is performed periodically between adjacent replicas according to a noise-aware test of acceptance. While its effectiveness on complex multimodal posteriors has been illustrated by testing over synthetic distributions, experiments on deep Bayesian neural network learning have shown its significant improvements over strong baselines for image classification.

#### 1 Introduction

Bayesian inference is one of the principled approaches to data analysis and provides a natural way of capturing the uncertainty within the quantities of interest [13]. A practical technique of posterior sampling in Bayesian inference is the Markov chain Monte Carlo methods [15]. Albeit successful in a wide-range of applications, the traditional MCMC methods, such as the Metropolis-Hastings (MH) algorithm [27, 17], the Gibbs sampler [14], and the hybrid/Hamiltonian Monte Carlo (HMC) [9, 30], have significant difficulties in dealing with complex probabilistic models with large datasets. The chief issues are two-fold: for complex models, there exists multiple modes, and some might be isolated with others such that the samplers might not be able to discover them, which leads to the *pseudo-convergence* [4]; for large datasets, the exploitation of mini-batches results in noise-corrupted gradient information that drives the sampler to deviate from the correct distributions [6].

To tackle the first fold of chief issues, some stochastic methods employing techniques stemmed in molecular dynamics have been proposed to alleviate the influence of mini-batch noise, e.g. the Stochastic Gradient Hamiltonian Monte Carlo [6] and the Stochastic Gradient Nosé-Hoover Thermostat [8]. These methods, however, still suffer from the pseudo-convergence problem. To address the second fold of chief issues, the idea of tempering [26, 10, 16] is conceived as a promising framework of solutions. It leverages the fact in statistical physics that a system at high temperature has a better chance to step across energy barriers between isolated modes of the state distribution [24] and hence enables rapid exploration. Although samplers based on tempering, such as the replicaexchange Monte Carlo [36], the simulated tempering [26] and the tempered transition [29], have shown improvements on complex distributions, the fact that they rely heavily on the exact evaluation of likelihood function, which is infeasible for large datasets, essentially prevents their application in large datasets. Notably, a recently proposed "thermostat-assisted continuous-tempered Hamiltonian Monte Carlo" (TACT-HMC) [25] has attempted to combine the advantage of molecular dynamics and tempering to address the issues of noise-corrupted gradient and pseudo-convergence. One major disadvantage of this method is that the procedure of continuous tempering keeps varying the effective temperature of the inner system; unbiased samples can only be generated when the inner system is at the unity temperature (which is a fraction of entire simulation interval). This means that its efficiency is relatively low and one has to run longer to obtain the same amount of effective samples.

<sup>\*</sup>Equal contribution; correspondence to: {r.luo,qiang.zhang}@cs.ucl.ac.uk.

To address together the issues of mini-batch gradient, pseudo-convergence and tempering efficiency, we propose a new sampler, Replica-exchange Nosé-Hoover Dynamics (RENHD). Our method simulates in parallel a collection of replicas with each at a different temperature. It automatically neutralizes the noise arising from mini-batch gradients, by equipping the Nosé-Hoover dynamics [11] for each replica. To alleviate pseudo-convergence, RENHD periodically swaps the configurations of replicas, during which a noise-aware test of acceptance is used to approximate the condition of detailed balance. As for tempering efficiency, our approach monitors in particular the replicas at unity temperature, which keeps generating unbiased samples; on the contrary, other tempered samplers, such as TACT-HMC [25], generates unbiased samples only in a fraction of running time, i.e. when the system stays at the unity temperature. Compared to the existing approaches, the novelty of RENHD lies in 1) it is the first replica-exchange method applicable to mini-batch settings 2) the integration of Nosé-Hoover dynamics with replica-exchange framework to enable continuous generation of unbiased samples from complex multimodal distributions; 3) the elaboration of the noise-aware exchange protocol with approximate Gaussian deconvolution, providing an analytical solution that improves the sampling precision and efficiency; 4) replica reduction with the "well-tempered ensemble" for very large systems to accelerate sampling and reduce resource usage without hurting performance. Experiments are conducted to validate the efficacy and demonstrate the effectiveness; it outperforms all baselines by a significant improvement on the accuracy of image classification with different types of neural network. Within the same simulation interval, RENHD maintains a higher maximum temperature and generates more than 4 times the size of samples.

# 2 Replica-exchange Nosé-Hoover Dynamics

This section serves as a straightforward description of our *Replica-exchange Nosé-Hoover Dynamics*. The proposed method contains two alternating subroutines, where the one in §2.1 simulates in parallel the Nosé-Hoover dynamics on a ladder of tempered replicas whereas the other one in §2.2 periodically exchanges the configurations between a pair of two replicas. An optional add-on is introduced in §2.3 for efficiency enhancement. A schematic illustration and more details can be found in Appendix A.

#### 2.1 Simulating replicas using the Nosé-Hoover dynamics with noisy gradient

Let  $\rho(\theta|\mathfrak{D})$  be the posterior distribution of the concerned variable  $\theta \in \mathbb{R}^d$  given the dataset  $\mathfrak{D} = \{x\}$ . With the prior distribution  $\rho(\theta)$  and likelihood function per datum  $\ell(\theta; x)$  that one determines a priori, the posterior can be calculated using Bayes' rule such that  $\rho(\theta|\mathfrak{D}) \propto \rho(\theta) \prod_{x \in \mathfrak{D}} \ell(\theta; x)$ .

A standard recipe for generating samples from  $\rho(\theta|\mathfrak{D})$  begins with establishing a mechanical system with a point mass moving in d-dimensional Euclidean space. The variable of interest  $\theta$  is now referred to as the system configuration, indicating the position of the particle. The target posterior transforms into the potential field  $U(\theta) \coloneqq -\log \rho(\theta|\mathfrak{D})$ , which determines the energy landscape of that system. Intuitively, the force induced by  $U(\theta)$  guides the motion of the particle, tracing out the trajectory  $\theta(t)$ ; the snapshots  $\{\theta_k\}$  registered periodically from  $\theta(t)$  will be tested and accepted as new samples.

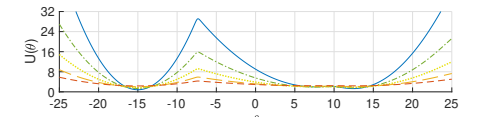
As the entire dataset  $\mathfrak D$  is involved in calculating the force  $f:=-\nabla U$ , it becomes computationally very expensive or even infeasible when  $\mathfrak D$  grows large. Therefore, for practical purpose, we resort to mini-batches  $\mathcal S \subset \mathfrak D$  for big datasets, which results in noisy estimates approximating the actual force

$$\tilde{f}(\theta) := \nabla \log \rho(\theta) + \frac{|\mathfrak{D}|}{|\mathcal{S}|} \sum_{x \in \mathcal{S}} \nabla \log \ell(\theta; x) \approx f(\theta). \tag{1}$$

It is clear that  $\tilde{f}$  is an unbiased estimator of f given the fact that each datum  $x \in \mathfrak{D}$  is *i.i.d.* Moreover, being sum of independent random variables,  $\tilde{f}$  converges to Gaussian in an asymptotic way as stated by the Central Limit Theorem (CLT). We assume  $\tilde{f}$ 's variance as constant due to its  $\theta$ -independence concluded in [5] and isotropic in all d dimensions for  $\theta$ 's symmetric nature as suggested in [8].

Now we construct an increasing ladder of temperatures  $\{T_j\}$ . On each rung j, we instantiate a replica of the physical system established previously. For each replica j, a set of dynamic variables is defined, which we refer to as the system state  $\Gamma_j = (\theta_j, p_j, \xi_j)$ , with  $p_j \in \mathbb{R}^d$  being  $\theta_j$ 's conjugate momentum and  $\xi \in \mathbb{R}$  denoting the Nosé-Hoover thermostat [31, 19] for adaptive noise dissipation [21]. There is a list of "replica-specific" constants to be assigned, namely the temperature  $T_j$ , the particle mass  $m_j$ , and the thermal inertia  $\kappa_j$ . The time evolution of  $\Gamma_j$  is governed by the Nosé-Hoover dynamics [11]:

$$\frac{\mathrm{d}\theta_j}{\mathrm{d}t} = \frac{p_j}{m_j}, \qquad \frac{\mathrm{d}p_j}{\mathrm{d}t} = \tilde{f}(\theta_j) - \xi_j p_j, \qquad \frac{\mathrm{d}\xi_j}{\mathrm{d}t} = \left[\frac{p_j^\mathsf{T} p_j}{m_j} - T_j d\right] \kappa_j, \tag{2}$$



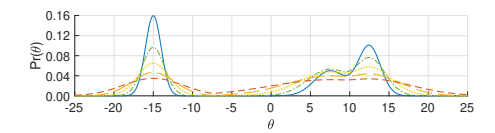


Figure 1: (*colored*) The *left* plot shows the effective potentials for 5 replicas at different temperatures. As temperature rises, the energy barrier at -7 reduces, which facilitates the passage. The right gives the corresponding marginal distributions, which move towards flattened histograms during tempering. The solid blue curves represent the real potential (*left*) and thus the true posterior (*right*) at T = 1.

where  $\tilde{f}$  represents the mini-batch approximation of the force, *i.e.* the gradient, as formulated in (1). The advantage of the Nosé-Hoover dynamics over the standard approach, Hamiltonian dynamics [30], is that the former can automatically recognize the noise within the gradient and adaptively neutralize its effect whereas the latter is likely to deviate from the correct distribution due to its vulnerability to noisy gradients. In contrast to the non-thermostatting proposals, *e.g.* SGMHC [6], the Nosé-Hoover thermostat saves us from manual noise estimation; it works properly with minimum prior knowledge. The following theorem validates the efficacy of the Nosé-Hoover dynamics in (2).

**Theorem 1.** The dynamics in (2) ensures the convergence of  $\Gamma_i$  to the unique invariant distribution

$$\pi_j(\Gamma_j) \propto e^{-\left[U(\theta_j) + p_j^{\top} p_j/2m_j\right]/T_j} \exp\left[-\frac{(\xi_j - B/m_j T_j)^2}{2\kappa_j T_j}\right]$$
 with the noise intensity  $B$ , (3)

*if the replica is ergodic.* 

*Proof.* The details can be found in Appendix B.

We simulate the time evolution of all replicas  $\{j\}$  in parallel using the dynamics in (2) until converged. A quick observation on (3) reveals the fact that all replicas share the same functional form of  $\pi_j(\Gamma_j)$ ; the difference between one invariant distribution and another is resulted from the different assignments of the replica-specific constants, especially the temperature. Considering replica j at temperature  $T_j$ , one can easily obtain the invariant distribution of  $\theta_j$  by marginalizing (3) w.r.t.  $p_j$  and  $\xi_j$ :

$$\pi_j(\theta_j) \propto \int \pi_j(\Gamma_j) \, \mathrm{d}p_j \, \mathrm{d}\xi_j \propto e^{-U(\theta_j)/T_j},$$
(4)

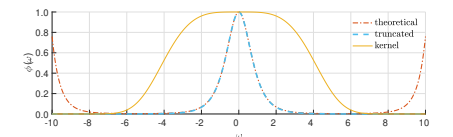
where the "effective" potential at  $T_j$  is essentially the actual potential U rescaled by a factor of  $1/T_j$ . Figure 1 shows the effective potentials of replicas at different temperatures; the corresponding  $\pi_j(\theta_j)$  are then illustrated. It becomes clear that when climbing the increasing ladder of temperatures  $\{T_j\}$ ,  $\pi_j(\theta_j)$  moves gradually towards a flat histogram. A physical interpretation is that the energy barriers separating isolated modes are effectively lowered and hence easier to overcome at high temperatures. Consequently, replicas at higher T's enjoy more efficient exploration of  $\theta$ -space. On the other hand, for "replica 0", i.e. the one at unity temperature  $T_0 = 1$ , the marginal  $\pi(\theta) \propto e^{-U(\theta)} \propto \rho(\theta|\mathfrak{D})$  restores the target posterior according to (4).

#### 2.2 Exchanging replicas using logistic test of acceptance with estimated potential differences

As we have investigated, replicas at high temperatures have better chances to transit between modes, leading to faster exploration of  $\theta$ -space. However, such advantage comes at a price that the sampling is no longer correct: the spectrum of sampled distribution widens in proportional to the square root of replica's temperature. This fact implies that the correct samples shall only be drawn from replica 0.

To enable rapid  $\theta$ -space exploration with high-temperature replicas whilst retaining accurate sampling, we develop a protocol that swaps the configurations between replicas systematically and periodically, and works well with mini-batches; the term "replica-exchange" refers to operations that swap  $\theta$ 's.

The protocol, as a non-physical probabilistic procedure, is built upon the principle of detailed balance, where every swap is equilibrated by its reverse counterpart. Such balance is maintained by a criterion with certain acceptance test; Baker's logistic test of acceptance [2] is utilized to assemble our protocol. As indicated by its name, this test relies on the logistic function  $g(z) = 1/[1 + e^{-z}]$ , and the potential difference  $\Delta E_{jk} := \left[U(\theta_j) - U(\theta_k)\right] \left[1/T_j - 1/T_k\right]$  between the pair of replicas (j,k) to be exchanged. The preference of Baker's test over its Metropolis counterpart comes from the super-smooth nature of the logistic function. Smoothness ensures the existence of smooth derivatives of infinite orders, which facilitates analytic formulations using infinite series, especially for problems involving deconvolutions.



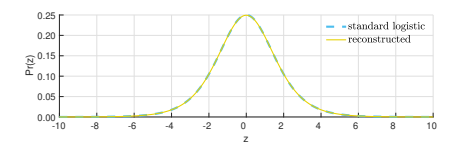


Figure 2: (*colored*) The *left* subplot shows the divergence (*red*) of density ratio in deconvoluting (6); a super-smooth kernel (*solid orange*) is applied to ensure convergence (*blue*). The *right* one compares the reconstructed (*solid yellow*) with the real (*dashed blue*); a good precision is achieved.

The Metropolis test, albeit more efficient, comprises non-smooth operations, min, which substantially sabotages the analyticity with a series of Delta functions arising from min's discontinuity.

When switching to mini-batches, the actual potential difference  $\Delta E_{jk}$  is no longer accessible; instead, we obtain a noisy estimate that approximates the actual value:

$$\Delta \tilde{E}_{jk} := \left[ \frac{1}{T_j} - \frac{1}{T_k} \right] \left[ \log \frac{\rho(\theta_j)}{\rho(\theta_k)} + \frac{|\mathfrak{D}|}{|\mathfrak{S}|} \sum_{x \in \mathfrak{S}} \log \frac{\ell(\theta_j; x)}{\ell(\theta_k; x)} \right] \approx \Delta E_{jk}, \tag{5}$$

which is essentially a random variable that converges asymptotically to Gaussian as indicated by CLT. As a result, the factorization  $\Delta \tilde{E}_{jk} = \Delta E_{jk} + z_N$  applies, where  $z_N \sim \mathcal{N}(0, \sigma^2)$  represents the random perturbation in the estimate from the underlying potential difference  $\Delta E_{jk}$ , with  $\sigma^2 := \mathbf{var}[\Delta \tilde{E}_{jk}]$ .

We introduce an auxiliary variable  $z_{\mathscr{C}}$  as suggested in [34]; its density  $q_{\mathscr{C}}$  is implicitly defined by

$$q_{\mathcal{L}}(z) = q_{\mathcal{C}}(z) * q_{\mathcal{N}_{\sigma^2}}(z), \text{ with } q_{\mathcal{L}}(z) = \frac{1}{(1 + e^{-z})(1 + e^z)}, \ q_{\mathcal{N}_{\sigma^2}}(z) = \frac{1}{\sqrt{2\pi\sigma^2}} \exp\left[-\frac{z^2}{2\sigma^2}\right],$$
 (6)

where  $q_{\mathcal{Z}}$  denotes the density of standard logistic distribution  $\mathcal{L}(0,1)$  and  $q_{\mathcal{N}_{\sigma^2}}$  is that of  $\mathcal{N}(0,\sigma^2)$ .

**Theorem 2.** The exchange of two replicas (j, k) approximately preserves detailed balance under the criterion that given  $\Delta \tilde{E}_{jk}$  evaluated by (5), we accept an attempt of swapping  $(\theta_i, \theta_k) \to (\theta_k, \theta_j)$  if

$$\Delta \tilde{E}_{jk} + z_{\mathcal{C}} > 0 \quad with \quad z_{\mathcal{C}} \sim \hat{q}_{\mathcal{C}}(z) := \sum_{n=0}^{\infty} \frac{(-\lambda)^n}{n!} H_n \left[ \frac{\mathbf{var}[\Delta \tilde{E}_{jk}]}{4\lambda} \right] \cdot q_{\mathcal{L}}^{(2n)}(z), \tag{7}$$

where  $H_n[\cdot]$  denotes the Hermite polynomials [1],  $q_{\mathcal{L}}^{(2n)}$  represents the 2n-th derivative of  $q_{\mathcal{L}}$  and  $\lambda$  is the "bandwidth" of kernel controlling the precision.

*Proof.* The details can be found in Appendix C.

Table 1: An example of Hermite polynomials and the derivatives of  $g(z) = 1/[1 + e^{-z}]$ .

order	$H_n\big[u=\sigma^2/4\lambda\big]$	$q_{\mathscr{L}}^{(2n)}(z)$ in terms of $g$
n = 0 $n = 1$ $n = 2$	$ \begin{array}{c c}  & 1 \\  & 2u \\  & 4u^2 & -2 \end{array} $	

#### Algorithm 1 The replica-exchange protocol

```
\Rightarrow \hat{q}_{\mathscr{C}} calculated using (7) with \sigma_*^2, \lambda
1: function EXCHANGE(\theta_i, \theta_k, model, \mathfrak{D}, |\mathcal{S}|_{\text{ex}}, \sigma_*^2, \lambda, \hat{q}_{\mathscr{C}})
2:
                     \mathcal{S} \leftarrow [\mathcal{S}, \text{NEXTBATCH}(\mathcal{D}, |\mathcal{S}|_{\text{ex}})]
3:
                                                                                                                                                                        > enlarging the mini-batch
4:
                     evaluate \Delta \tilde{E} using (5) with \delta, model.\rho() and model.\ell()
              until var[\Delta \tilde{E}] < \sigma_*^2
5:
              z_{\mathcal{N}_*} \sim \mathcal{N}(0, \sigma_*^2 - \Delta \tilde{E})
z_{\mathcal{C}} \sim \hat{q}_{\mathcal{C}}
                                                                                                                                                                  ▶ z_{\mathcal{N}_*} ensuring variance ≈ \sigma_*^2
6:
                                                                                                                                                              ▶ using Gibbs sampler or HMC
7:
              if \Delta \tilde{E} + z_{\mathcal{N}_*} + z_{\mathscr{C}} > 0 then:

(\theta_j, \theta_k) \leftarrow (\theta_k, \theta_j)
8:
                                                                                                                                                                              > checking the criterion
9:
                                                                                                                                                                         ▶ swapping configurations
```

A nice property of the logistic derivatives is that all  $q_{\mathcal{L}}^{(2n)}$  can be formulated as polynomials in terms of the logistic function g with coefficients extracted from the *Worpitzky Triangle*. We express the first three logistic derivatives of even order in Table 1; for any  $q_{\mathcal{L}}^{(2n)}$ , the highest order of g-terms is 2n + 2.



Figure 3: Effect of deploying WTE on a set of 5 replicas at different temperatures. On the *left* depicts the real histograms of replicas' energy distributions while the *right* shows their tempered counterparts. With WTE enabled, the energy overlap (*shaded*) of adjacent replicas is greatly enlarged, which leads to a better chance for successful exchange and therefore a higher efficiency.

The coefficient of the k-th g-term in  $q_{\mathcal{L}}^{(2n)}$  is essentially W(2n,k) of the triangle. A recursive routine is provided as an alternative in [28].

In practice, we precalculate  $\hat{q}_{\mathscr{C}}$  using (7) with a constant tolerance  $\sigma_*^2$  and a sufficiently small  $\lambda$ ; for arbitrary precision, the infinite series can be truncated at an appropriate level for a finite summation. Figure 2 demonstrates the approximation by only a handful of derivatives  $q_{\mathscr{L}}^{(2n)}$ ; comparison is made between the real standard logistic  $q_{\mathscr{L}}$  and the reconstructed  $\hat{q}_{\mathscr{C}} * q_{\mathcal{N}_{\sigma^2}}$ , indicating a perfect precision.

For an attempt of swapping, we make sure  $\mathbf{var}[\Delta \tilde{E}_{jk}] < \sigma_*^2$  and sample a new Gaussian  $z_{\mathcal{N}_*}$  such that the variance of sum  $\mathbf{var}[\Delta \tilde{E}_{jk} + z_{\mathcal{N}_*}] \approx \sigma_*^2$ . When validating the criterion,  $\hat{q}_{\mathscr{C}}$  is reused for sampling the *correction variable*  $z_{\mathscr{C}}$  as the density is retained in the memory; conventional samplers, such as the Gibbs sampler [14] and HMC [30], can be leveraged. The protocol is formalized as Algorithm 1.

In comparison with the numerical treatment in [34], our approach provides an analytic approximation to the ill-defined Gaussian decovolution corresponding to the mini-batch replica-exchange protocol. Given an arbitrary precision, one can readily re-evaluate the approximation for the expected precision using Table (1), instead of invoking the entire numerical procedure. Empirical evaluation demonstrates that a significant improvement ( $20 \times boost$ ) on efficiency can be guaranteed in sampling the correction distribution using our analytic approach with the Gibbs sampler; the numerical solution in comparison uses the pre-computed density<sup>2</sup> and the conventional methods, namely binary search and hash tables.

#### 2.3 Reducing replicas using the Well-tempered Ensemble

In this subsection, we discuss an "optional" device, the *Well-tempered Ensemble* [3], for our RENHD. WTE is important, albeit not indispensable, for its use of enhancing the memory efficiency of RENHD by reducing the number of replicas for real-world applications, especially for deep neural networks.

Intuitively, the efficiency of RENHD relies on the chance of successful swaps, and the latter is merely a function of (potential) energy differences: in §2.2, the acceptance probability is of the form  $g(\Delta E_{jk})$ . For a pair of replicas (j, k), a greater overlap of the energy distributions  $\pi_j(E)$  and  $\pi_k(E)$  will lead to a better chance on the exchange between  $\theta_j$  and  $\theta_k$ . However, observations reveal that the overlap will decrease in the rate of  $1/\sqrt{d}$  when the system size d (i.e. the dimension for  $\theta \in \mathbb{R}^d$ ) increases [10]. Therefore, to retain a constant acceptance probability, the number of replicas needs to increase in  $\sqrt{d}$ . For very large systems such as deep neural networks, the amount might be prohibitively large.

WTE manages to reduce the replicas number by enlarging the energy overlap of replicas. It constructs and then maintains for each replica j a time-dependent biasing potential  $A_j^{\gamma}(E,t)$  with  $\gamma > 1$  denoting the *tempering factor*, which is a predefined constant defining the increase of energy overlaps by WTE. Figure 3 illustrates the effect of deploying WTE on a demo model with Gaussian energy distributions; the overlap of energy distributions (of adjacent replicas) is substantially enlarged.

The time evolution of the biasing potential  $A_i^{\gamma}$  in WTE is defined by

$$\frac{\mathrm{d}A_{j}^{\gamma}(E,t)}{\mathrm{d}t} = h \exp\left[-\frac{A_{j}^{\gamma}(E,t)}{(\gamma-1)T_{j}}\right] \cdot \delta\left[E - U(\theta_{j}(t))\right],\tag{8}$$

where  $\theta_j(t)$  indicates the trajectory of  $\theta_j$  at time t, h is a constant determining the learning rate of  $A_j^{\gamma}$ , and  $\delta[\cdot]$  denotes the Dirac delta function. As  $\gamma$  is a constant, we hereafter omit it for simplicity. It has been shown that  $A_j(E,t)$  converges asymptotically [7]. With  $A_j(E) := A_j(E,t \to \infty)$ , the augmented

<sup>&</sup>lt;sup>2</sup>https://github.com/BIDData/BIDMach

#### Algorithm 2 Replica-exchange Nosé-Hoover dynamics with well-tempered ensemble

```
1: function NHDYNAMICS(\{\theta_j\}, \{A_j[\cdot]\}, \{T_j\}, model, \mathfrak{D}, |\mathcal{S}|_{\mathrm{nhd}}, N, \epsilon, \mu, c, \gamma, h, \Delta)
                                                                                   ▶ NHD length N; \epsilon, \mu, c in (13); \gamma, h in (8); \Delta for quantizing A_i
 2:
 3:
              for all \{j\} do
                                                                                                                                                       ▶ all j running in parallel
 4:
                    v_i \sim \mathcal{N}(0, T_i \epsilon) and s_i \leftarrow c/T_i
                                                                                                                                               ▶ resetting auxiliary variables
  5:
                    for n = RANGE(1, N) do
 6:
                           \mathcal{S} \leftarrow \text{NEXTBATCH}(\mathcal{D}, |\mathcal{S}|_{\text{nhd}})
                                                                                                                                                      ▶ fetching new mini-batch
 7:
                           E_j \leftarrow \text{model.FORWARD}(\theta_j, \mathcal{S})
                                                                                                                                                                           \triangleright E_j := U(\theta_j)
                           \hat{f_j} \leftarrow \text{model.BACKWARD}(\theta_j, \delta)

i \leftarrow \text{QUANTIZE}(E_j)

dA_j \leftarrow \left[A_j[i+1] - A_j[i]\right]/\Delta
 8:
                                                                                                                                          ▶ evaluating mini-batch gradient
 9:
                                                                                                                                        \triangleright indexing A_i[i] for quantized E_i
10:

ightharpoonup approximating dA_j(E)/dE
                           \begin{aligned} & dV_j \leftarrow \begin{bmatrix} 1 + dA_j \end{bmatrix} \tilde{f_j} \\ & v_j \leftarrow v_j + dV_j \epsilon - s_j v_j + \mathcal{N}(0, 2c\epsilon) \\ & \theta_j \leftarrow \theta_j + v_j \text{ and } s_j \leftarrow s_j + \mu \left[ v_j^\top v_j / d - T_j \epsilon \right] \end{aligned}
                                                                                                                                                    \triangleright V_i := U(\theta_i) + A_i(U(\theta_i))
11:
                                                                                                                                       ▶ additional Gaussian noise added
12:
13:
                                                                                                                                                        ▶ simulating NHD in (2)
                           A_i[i] \leftarrow A_i[i] + h \exp \left[ -A_i[i]/(\gamma - 1)T_i \right]
14:
                                                                                                                                                        \triangleright updating A_i[\cdot] cf. (14)
              return \{\theta_i\}, \{A_i[\cdot]\}
15:
16: MAIN:
17: \{\theta_i\} \leftarrow \text{RANDN}() and \{A_i[\cdot]\} \leftarrow \text{ZEROS}()
                                                                                                                                                                          ▶ initialization
18: args \leftarrow (|\mathcal{S}|_{nhd}, N, \epsilon, \mu, c, \gamma, h, \Delta)
                                                                                                                                                              ▶ packing arguments
19: loop
              \{\theta_i\}, \{A_i[\cdot]\} \leftarrow \text{NHDYNAMICS}(\{\theta_i\}, \{A_i[\cdot]\}, \{T_i\}, \text{model}, \mathcal{D}, \text{args})
20:
21:
              \{(j,k)\} \leftarrow \text{RAND}()
                                                                                                                                    ▶ sampling a set of replicas to swap
22:
              for all \{(j, k)\} do
23:
                     REPLICAEXCHANGE(\theta_i, \theta_k, \text{model}, \mathfrak{D}, |\mathcal{S}|_{\text{re}}, \sigma_*^2, \lambda, \hat{q}_{\mathscr{C}})
                                                                                                                                                                ▶ recall Algorithm 1
24:
                     if \theta_i and \theta_k exchanged then swap A_i[\cdot] and A_k[\cdot]
25:
              samples \leftarrow [samples, \theta_0]
                                                                                                                             ▶ reweighting needed using (11) or (12)
```

potential can be defined as  $V_i(\theta_i) := U(\theta_i) + A_i(U(\theta_i))$  and the tempered energy distribution reads

$$\tilde{\pi}_{j}^{A}(E) \propto \int \delta \left[ E - U(\theta_{j}) \right] e^{-V(\theta_{j})/T_{j}} d\theta_{j} = \left( \int \delta \left[ E - U(\theta_{j}) \right] d\theta_{j} \right) e^{-\left[ E + A_{j}(E) \right]/T_{j}}. \tag{9}$$

**Theorem 3.** The energy distribution (9) of the WTE-augmented replica j with converged  $A_j$  satisfies

$$\tilde{\pi}_j^A(E) \propto \left[\pi_j(E)\right]^{1/\gamma},$$
(10)

indicating that the fluctuation  $\mathbf{var}[E]$  w.r.t.  $\tilde{\pi}_i^A$  is effectively amplified by a factor  $\gamma$ .

*Proof.* The details can be found in Appendix D.

The marginal distribution of  $\theta_i$  for the WTE-augmented replica j is then modified as (cf. (4))

$$\tilde{\pi}_j^A(\theta_j) \propto e^{-V_j(\theta_j)/T_j} = \exp\left[-\frac{U(\theta_j) + A_j(U(\theta_j))}{T_j}\right] \propto \pi_j(\theta_j) e^{-A_j(U(\theta_j))/T_j},\tag{11}$$

which deviates from the concerned marginal  $\pi_j(\theta_j)$  in (4) by a factor  $e^{-A_j(U(\theta_j))/T_j}$ . A re-weighting procedure needs to be conducted by simply implementing importance sampling with the same factor. In practical scenarios where WTE is deployed, large models, *e.g.* deep neural networks, often involve; it is usually the canonical average of some function  $r(\theta_j)$ , *i.e.* its Monte Carlo integration *w.r.t.*  $\pi_j(\theta_j)$ , rather than the posterior distribution  $\rho(\theta|\mathfrak{D}) \equiv \pi(\theta|T=1)$  itself that really matters. For that average, we can readily evaluate it in a simple and unbiased way derived from (11):

$$\langle r(\theta_j) \rangle_{\pi_j} = \frac{\left\langle r(\theta_j) e^{A_j(U(\theta_j))/T_j} \right\rangle_{\tilde{\pi}_j^A}}{\left\langle e^{A_j(U(\theta_j))/T_j} \right\rangle_{\tilde{\pi}_j^A}}, \text{ with samples drawn from } \tilde{\pi}_j^A, \tag{12}$$

where the biasing potential  $A_i(U(\theta_i))$  can be evaluated on the fly during the simulation.

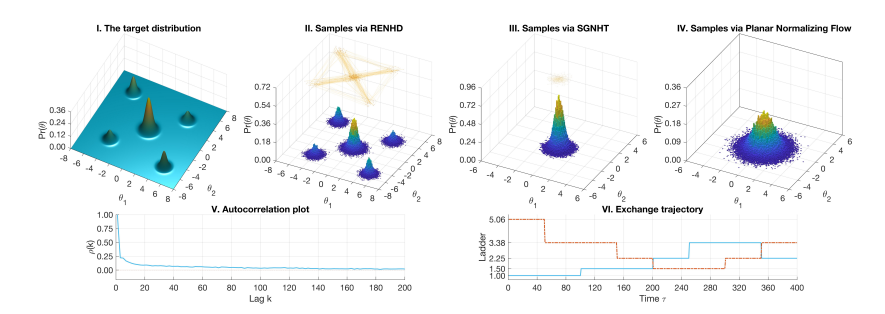


Figure 4: Experiment on sampling a 2d mixture of 5 Gaussians.

# 3 Implementation

This section is devoted to the implementation of the proposed sampler, RENHD, in practical scenarios. Particular attention is paid to the discretization of the continuous-time dynamics in (2) and (8).

Let us begin with discretizing the Nosé-Hoover dynamics in (2). With non-vanishing time steps  $\Delta t$ , we make a change of variables by defining for each replica j:

the variables 
$$v_j := \frac{p_j \Delta t}{m}$$
,  $s_j := \xi_j \Delta t$  and the constants  $\epsilon := \frac{\Delta t^2}{m}$ ,  $\mu := m\kappa d$ ,  $c := \frac{C\Delta t}{m}$ , (13)

where the particle mass m as well as the thermal inertia  $\kappa$  are set equal for all replicas, and the newly introduced constant  $c_j$  defines additional Gaussian noise with a predefined intensity  $C \approx 20B$  in (3) to enhance the ergodicity. As suggested in [23], the temperature ladder  $\{T_j\}$  is defined geometrically as a series:  $T_j = \tau^j$  with  $\tau > 1$  being the constant ratio for all j = 0, 1, 2, ..., M.

Now we devise WTE's update rule for replica j by setting an array to restore the biasing potential  $A_j$ . Given the granularity  $\Delta$ , the energy E is quantized; each segment is then associated to one of the cells in that array.  $A_j$  is evaluated for all quantized E, with the values registered in the corresponding cells. Time is discretized  $t \to n\Delta t$  using the same steps; the differential equation (8) is hence converted into

$$A_{j}[E;n] \leftarrow A_{j}[E_{j};n-1] + h \,\delta_{E,E_{j}^{(n)}} \exp\left[-\frac{A_{j}[E_{j}^{(n)};n-1]}{(\gamma-1)T_{j}}\right],\tag{14}$$

where the learning rate h controls the size of increments,  $\delta_{E,E_j^{(n)}}$  defines the Kronecker delta function in the quantized E while  $E_j^{(n)} \coloneqq U(\theta_j(n\Delta t))$  denoting the potential energy evaluated at the n-th step. By initializing  $A_j[E;0] \equiv 0$ , the biasing potential is adaptively accumulated through the simulation. Algorithm 2 provides a procedural description of RENHD with WTE deployed; an alternative version of RENHD without WTE can be found in Appendix E.

#### 4 Experiment

We conduct two sets of experiments: the first uses synthetic scenarios, verifying the desired properties of our method; the second is on real datasets, showing a significant improvement against baselines.

#### 4.1 Synthetic distributions

To verify the efficacy of RENHD, we perform a sampling test on a synthetic 2d Gaussian mixture with 5 isolated modes. The potential energy and its gradient is perturbed by zero-mean Gaussian noise with variance  $\sigma^2 = 0.25$  which stays unknown for samplers. A temperatures ladder is established with 7 rungs and the geometric factor  $\tau = 1.5$ ; the temperature ranges from  $T_0 \equiv 1$  to  $T_7 = (1.5)^7 \approx 11.4$ . We compare the sampled histogram with the non-tempered sampler, SGNHT [8], and a typical variational inference method, the plannar Normalizing Flow [32]. Figure 4 demonstrates that REHND has accurately sampled the target multimodal distribution in the presence of mini-batch noise. On the contrary, SGNHT and PNF failed to discover the isolated modes; the latter deviates severely due to the noise, resulting in a spread histogram. We have depicted the sampling trajectory above for the samplers, which indicates a good mixing property of RENHD against SGNHT. Moreover, we provide the autocorrelation plot for RENHD's samples and illustrate the history of swaps between replicas within a short interval of simulation. The effective sample size of RENHD is  $4.1638 \times 10^3$  out of  $10^5$ .

Table 2: Result of Bayesian learning experiments on real datasets.

	RNN on Fashion-MNIST			CNN on CIFAR-10		
% permuted labels	0 %	20 %	30 %	0 %	20 %	30 %
Adam [22] momentum [35] SGHMC [6] SGNHT [8] TACT-HMC [25]	88.56 ± 0.13 % 88.83 ± 0.11 % 89.12 ± 0.12 % 89.23 ± 0.18 % 89.74 ± 0.13 %	87.93 ± 0.18 % 88.15 ± 0.19 % 88.23 ± 0.16 % 88.26 ± 0.22 % 88.83 ± 0.17 %	87.22 ± 0.23 % 87.58 ± 0.20 % 87.79 ± 0.19 % 87.74 ± 0.19 % 88.78 ± 0.17 %	71.94 ± 0.13 % 65.86 ± 0.13 % 75.84 ± 0.11 % 76.70 ± 0.09 % 78.23 ± 0.10 %	71.88 ± 0.20 % 66.84 ± 0.19 % 72.50 ± 0.18 % 73.83 ± 0.19 % 74.22 ± 0.16 %	$70.93 \pm 0.25 \%$ $67.84 \pm 0.23 \%$ $71.15 \pm 0.25 \%$ $71.79 \pm 0.24 \%$ $73.34 \pm 0.22 \%$
RENHD in Alg. 2	90.87 ± 0.12 %	89.45 ± 0.17 %	89.06 ± 0.16 %	79.65 ± 0.11 %	75.43 ± 0.17 %	<b>74.02</b> ± 0.23 %

#### 4.2 Bayesian learning on real image datasets with convolutional and recurrent neural nets

We conduct image classification on two real datasets: Fashion-MNISTand CIFAR-10each on a typical recurrent neural network (RNN) and a convolutional neural network (CNN), respectively. The performance is evaluated and compared in terms of the accuracy of classification. The recent TACT-HMC [25] as well as two classic mini-batch-compatible samplers, i.e. SGNHT [8] and SGHMC [6], are chosen as part of the baselines; besides, two widely-used gradient-based optimisers, Adam [22] and momentum SGD [35], are compared. Note that the algorithms relating Normalizing Flow are not compared, since these NF-based methods are impractical in sampling high-dimensional  $\theta$ -space. All four baselines are tuned to their best on each task; the samplers' accuracy of classification is calculated from Monte Carlo integration on sampled models; the optimizers are evaluated on test sets.

For all methods, every single run composes 1000 epochs in either sampling or training before the final evaluation. We randomly permute a certain percentage (0%, 20%, and 30%) of the training labels at the beginning of each epoch as suggested in [25]. We use  $|\mathcal{S}|_{\text{hhd}} = 128$  for the parallel evolution and  $|\mathcal{S}|_{\text{re}} = 256$  for the replica exchange. The additional noise level is fixed at c = 0.1. The geometric temperature ladders is setup with 12 rungs and the ratio  $\tau = 1.2$ , leading to a highest temperature at  $(1.2)^{12} \approx 9$ . WTE is enabled with  $\gamma = 2$ , h = 0.0001,  $\Delta = 0.1$ . The swap is attempted after every 40 effective samples obtained. The step size  $\epsilon = 5 \times 10^{-6}$ , the thermal inertia  $\mu = 1$  and the length of simulating trajectory N = 200. The bandwidth  $\lambda = 0.05$  and the reference variance  $\sigma_*^2 = 0.5$ .

**Fashion-MNIST classification with RNN.** The RNN is composed of one LSTM layer [18] as the first layer, with the input/output dimensions of 28/128. It takes as the input via scanning a  $28 \times 28$  image vertically each line of a time. After 28 scanning steps, the LSTM outputs a representative vector of size 128 into ReLU activation, which is followed by a dense layer of size 64 with ReLU activation. The prediction on 10 categories is generated by softmax activation in the output layer.

**CIFAR-10 classification with CNN.** The CNN contains four learnable layers: from the bottom to the top, a 2d conv layer using the kernel of size  $3 \times 3 \times 16$ , and another 2d conv layer with the kernel of size  $3 \times 3 \times 16 \times 16$ , then two dense layers of size 80 and 10. ReLU activations are inserted between each of those learnable layers. For each conv layer, the stride is set to  $1 \times 1$ , and a pooling layer with  $2 \times 2$  stride is appended after the ReLU activation. Softmax is used for the final prediction.

**Discussion.** RENHD outperforms all classic baselines with a relatively large margin due to the incorporation of tempering. In the comparison with TACT-HMC, another tempering-enhanced sampler, RENHD still maintains better performance. Moreover, RENHD is devised with much simpler dynamics and fewer hyperparameters, reducing 60% computation for one step of simulation compared with TACT-HMC and greatly simplifying debugging or tuning. It can constantly generate valid samples while using TACT-HMC one has only 18% chances to get a valid one. Hence, we believe that RENHD is of much more practical interest for its virtue of easy implementation, fast deployment, and high efficiency. The result is summarized in Table 2, where the average accuracy of classification is reported, with a variation calculated from 10 independent runs in each setting.

#### 5 Conclusion

We propose a new sampler, RENHD, as the first replica-exchange method applicable to mini-batch settings, which can efficiently draw representative samples from complex posterior distributions with multiple isolated modes in the presence of mini-batch noise. It simulates a ladder of replicas in different temperatures, and alternating between subroutines of evolving the Nosé-Hoover dynamics using the mini-batch gradient and performing configuration exchange based on noise-aware acceptance test. Experiments are conducted to validate the efficacy and demonstrate the effectiveness; it outperforms all baselines compared by a significant improvement on the accuracy of image classification with different types of neural network. The results have demonstrated the potential of facilitating deep Bayesian learning on large datasets where multimodal posteriors and mini-batch gradient exist.

#### References

- [1] Milton Abramowitz and Irene A Stegun. *Handbook of mathematical functions: with formulas, graphs, and mathematical tables,* volume 55. Courier Corporation, 1965.
- [2] Av A Barker. Monte carlo calculations of the radial distribution functions for a proton-electron plasma. *Australian Journal of Physics*, 18(2):119–134, 1965.
- [3] Massimiliano Bonomi and Michele Parrinello. Enhanced sampling in the well-tempered ensemble. *Physical review letters*, 104(19):190601, 2010.
- [4] Steve Brooks, Andrew Gelman, Galin Jones, and Xiao-Li Meng. *Handbook of markov chain monte carlo*. CRC press, 2011.
- [5] Pratik Chaudhari and Stefano Soatto. Stochastic gradient descent performs variational inference, converges to limit cycles for deep networks. In 6th International Conference on Learning Representations, ICLR 2018, Vancouver, BC, Canada, April 30 May 3, 2018, Conference Track Proceedings. OpenReview.net, 2018.
- [6] Tianqi Chen, Emily B Fox, and Carlos Guestrin. Stochastic gradient hamiltonian monte carlo. In *ICML*, pages 1683–1691, 2014.
- [7] James F Dama, Michele Parrinello, and Gregory A Voth. Well-tempered metadynamics converges asymptotically. *Physical review letters*, 112(24):240602, 2014.
- [8] Nan Ding, Youhan Fang, Ryan Babbush, Changyou Chen, Robert D Skeel, and Hartmut Neven. Bayesian sampling using stochastic gradient thermostats. In *Advances in neural information processing systems*, pages 3203–3211, 2014.
- [9] Simon Duane, Anthony D Kennedy, Brian J Pendleton, and Duncan Roweth. Hybrid monte carlo. *Physics letters B*, 195(2):216–222, 1987.
- [10] David J Earl and Michael W Deem. Parallel tempering: Theory, applications, and new perspectives. *Physical Chemistry Chemical Physics*, 7(23):3910–3916, 2005.
- [11] Denis J Evans and Brad Lee Holian. The nose–hoover thermostat. *The Journal of chemical physics*, 83(8):4069–4074, 1985.
- [12] Jianqing Fan. On the optimal rates of convergence for nonparametric deconvolution problems. *The Annals of Statistics*, pages 1257–1272, 1991.
- [13] Andrew Gelman, Hal S Stern, John B Carlin, David B Dunson, Aki Vehtari, and Donald B Rubin. *Bayesian data analysis*. Chapman and Hall/CRC, 2013.
- [14] Stuart Geman and Donald Geman. Stochastic relaxation, gibbs distributions, and the bayesian restoration of images. *IEEE Transactions on pattern analysis and machine intelligence*, 6(6):721–741, 1984.
- [15] Walter R Gilks, Sylvia Richardson, and David Spiegelhalter. *Markov chain Monte Carlo in practice*. Chapman and Hall/CRC, 1995.
- [16] Gianpaolo Gobbo and Benedict J Leimkuhler. Extended hamiltonian approach to continuous tempering. *Physical Review E*, 91(6):061301, 2015.
- [17] W Keith Hastings. Monte carlo sampling methods using markov chains and their applications. *Biometrika*, 57(1):97–109, 1970.
- [18] Sepp Hochreiter and Jürgen Schmidhuber. Long short-term memory. *Neural computation*, 9(8):1735–1780, 1997.
- [19] William G Hoover. Canonical dynamics: equilibrium phase-space distributions. *Physical review A*, 31(3):1695, 1985.
- [20] AF Jones and DL Misell. A practical method for the deconvolution of experimental curves. *British Journal of Applied Physics*, 18(10):1479, 1967.
- [21] Andrew Jones and Ben Leimkuhler. Adaptive stochastic methods for sampling driven molecular systems. *The Journal of chemical physics*, 135(8):084125, 2011.
- [22] Diederik P. Kingma and Jimmy Ba. Adam: A method for stochastic optimization. *CoRR*, abs/1412.6980, 2014.
- [23] David A Kofke. On the acceptance probability of replica-exchange monte carlo trials. *The Journal of chemical physics*, 117(15):6911–6914, 2002.

- [24] Lev Davidovich Landau and Evgenii Mikhailovich Lifshitz. Course of theoretical physics. Elsevier, 2013.
- [25] Rui Luo, Yaodong Yang, Jun Wang, and Yuanyuan Liu. Thermostat-assisted continuously-tempered hamiltonian monte carlo for multimodal posterior sampling on large datasets. In *Advances in Neural Information Processing Systems*, 2018.
- [26] Enzo Marinari and Giorgio Parisi. Simulated tempering: a new monte carlo scheme. *EPL* (*Europhysics Letters*), 19(6):451, 1992.
- [27] Nicholas Metropolis, Arianna W Rosenbluth, Marshall N Rosenbluth, Augusta H Teller, and Edward Teller. Equation of state calculations by fast computing machines. *The journal of chemical physics*, 21(6):1087–1092, 1953.
- [28] Ali A Minai and Ronald D Williams. On the derivatives of the sigmoid. *Neural Networks*, 6(6):845–853, 1993.
- [29] Radford M Neal. Sampling from multimodal distributions using tempered transitions. *Statistics and computing*, 6(4):353–366, 1996.
- [30] Radford M Neal. MCMC using Hamiltonian dynamics. *Handbook of Markov Chain Monte Carlo*, 2:113–162, 2011.
- [31] Shuichi Nosé. A unified formulation of the constant temperature molecular dynamics methods. *The Journal of chemical physics*, 81(1):511–519, 1984.
- [32] Danilo Rezende and Shakir Mohamed. Variational inference with normalizing flows. In *International Conference on Machine Learning*, pages 1530–1538, 2015.
- [33] H. Risken and H. Haken. *The Fokker-Planck Equation: Methods of Solution and Applications Second Edition*. Springer, 1989.
- [34] Daniel Seita, Xinlei Pan, Haoyu Chen, and John F. Canny. An efficient minibatch acceptance test for metropolis-hastings. In *Proceedings of the Thirty-Third Conference on Uncertainty in Artificial Intelligence, UAI 2017, Sydney, Australia, August 11-15, 2017, 2017.*
- [35] Ilya Sutskever, James Martens, George Dahl, and Geoffrey Hinton. On the importance of initialization and momentum in deep learning. In *International conference on machine learning*, pages 1139–1147, 2013.
- [36] Robert H Swendsen and Jian-Sheng Wang. Replica monte carlo simulation of spin-glasses. *Physical Review Letters*, 57(21):2607, 1986.

# Supplementary Information of #3793 "Replica-exchange Nosé-Hoover dynamics for Bayesian learning on large datasets" at NeurIPS 2019

#### A A systematic illustration of the proposed method

The proposed method contains two alternating subroutines: 1. dynamics evolution of all system replicas in parallel, and 2. configuration exchange between adjacent replicas where the condition of detailed balance is met. The first subroutine exploits the Nosé-Hoover dynamics [11] to determine and adaptively neutralize the noise arising from mini-batch gradients; the second leverages a specific logistic test of acceptance that is well-functioning with mini-batches, to preserve detailed balance during each exchange. Figure 5 demonstrates the runtime trajectories of 5 replicas, in which two subroutines are invoked in an alternative scheme. In the following subsections, theoretical bases will be established.

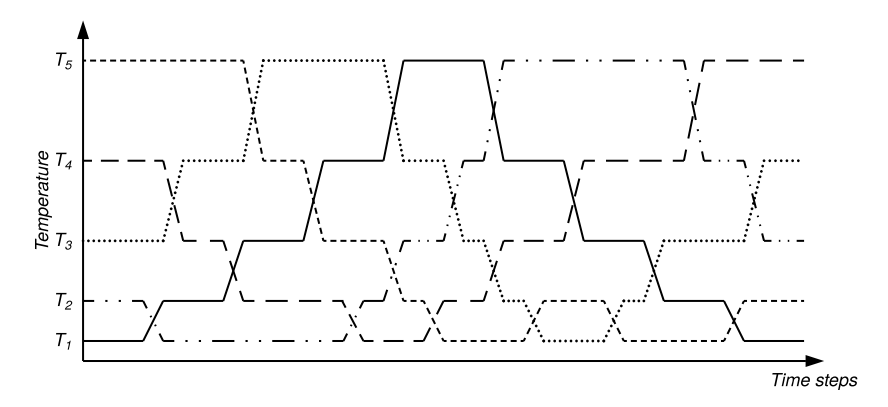


Figure 5: A schematic demonstration of replica-exchange protocol. It comprises two alternating subroutines: 1. dynamics evolution of all replicas in parallel; 2. configuration exchange between adjacent replicas with the detailed balance. Lines describe 5 trajectories of dynamics of replicas at different temperatures: horizontal segments represent parallel evolution while intersections between endpoints denote configuration exchange.

#### B Proof of Theorem 1

*Proof.* We prove the existence of the invariant distributions. The uniqueness follows as a consequence of the assumption on ergodicity.

The Nosé-Hoover dynamics in (2) defines a system of stochastic differential equations, which governs the time evolution of state in a probabilistic way from a microscopic perspective. On the other hand, consider the entire ensemble, i.e. the collection of all possible states, its evolution can be characterized statistically from a macroscopic point of view through the time evolution of state distribution  $\pi_j(\Gamma_j, t)$ . The Fokker-Planck equation [33] translates the stochastic dynamics of state into the differential equation

$$\dot{\pi}_{j}(\Gamma_{j},t) = -\partial_{\theta_{j}}^{\top} \left[ (p_{j}/m_{j})\pi_{j} \right] - \partial_{p_{j}}^{\top} \left[ f(\theta_{j})\pi_{j} \right] + \partial_{p_{j}}^{\top} \left[ \xi_{j} p_{j} \pi_{j} \right] 
- \partial_{\xi_{j}} \left[ (p_{j}^{\top} p_{j}/m_{j} - T_{j} d)\kappa_{j}\pi_{j} \right] + \partial_{p_{j}}^{\top} \left[ B \partial_{p_{j}} \pi_{j} \right],$$
(15)

which can be solved deterministically or even analytically; the invariant distributions can be indicated by  $\dot{\pi}_j(\Gamma_j, t) = 0$ .

We presume that the invariant distribution of  $\xi$  is separable from that of  $\theta_j$  and  $p_j$  so that  $\pi_j(\Gamma_j) = \pi_j(\xi_j)\pi_j(\theta_j, p_j)$ . For the marginal distribution  $\pi_j(\theta_j, p_j)$ , we consider the typical Boltzmann distribution for the Hamiltonian system  $(\theta_j, p_j)$  with the potential U and an additive quadratic kinetic energy  $p_j^{\mathsf{T}} p_j/2m_j$  as is defined for our system:

$$\pi_j(\theta_j, p_j) \propto \exp\left[-\left[U(\theta_j) + p_j^{\top} p_j/2m_j\right]/T_j\right].$$
 (16)

When solving  $\dot{\pi}_j(\Gamma_j, t) = 0$ , the Boltzmann  $\pi_j(\theta_j, p_j)$  in (16) results in the Hamiltonian dynamics [30]; the first and second terms in (15) therefore cancel with each other. The resulting equation w.r.t.  $\pi_j(\xi_j)$  is simplified as

$$\frac{1}{\pi_j(\xi_j)}\frac{\mathrm{d}\pi_j(\xi_j)}{\mathrm{d}\xi_j} = -\frac{1}{\kappa_j T_j} \bigg[ \xi_j - \frac{B}{m_j T_j} \bigg],$$

which gives the unique solution up to a normalizing constant

$$\pi_j(\xi) \propto \exp\left[-\frac{(\xi_j - B/m_j T_j)^2}{2\kappa_j T_j}\right].$$
 (17)

Combining two marginal distributions in (16) and (17), the joint distribution of state is obtained as in (3), which is invariant by construction.

#### C Proof of Theorem 2

*Proof.* We start with the investigation on a simple system of two replicas, namely (j, k); any composite system with a number of replicas simply extends the basic scenario, because every swap takes place between a pair of replicas.

For that 2-replica system to satisfy detailed balance during replica exchange, the relation below holds

$$\pi_{i}(\theta_{i})\pi_{k}(\theta_{k})\alpha_{jk}\left[(\theta_{i},\theta_{k})\to(\theta_{k},\theta_{i})\right] = \pi_{i}(\theta_{k})\pi_{k}(\theta_{i})\alpha_{jk}\left[(\theta_{k},\theta_{i})\to(\theta_{i},\theta_{k})\right],\tag{18}$$

where  $\pi_j(\theta_j)$  represents the marginal distribution of replica j's current configuration  $\theta_j$  as formulated in (4), and  $\alpha_{jk} \left[ (\theta_j, \theta_k) \to (\theta_k, \theta_j) \right]$  denotes the acceptance probability of the pair (j, k) moves from the initial setting the initial setting  $(\theta_j, \theta_k)$  to the final setting  $(\theta_k, \theta_j)$ . Note that  $\theta_j$  indicates only the value of j's configuration at the particular time instance; after switching, j's configuration becomes  $\theta_k$ , i.e. swapped with k's.

The acceptance probability of Baker's test reads

$$\alpha_{jk}^{\mathrm{B}}\left[(\theta_{j},\theta_{k})\to(\theta_{k},\theta_{j})\right] \coloneqq \frac{1}{1+\left[\pi_{j}(\theta_{j})\pi_{k}(\theta_{k})\right]/\left[\pi_{j}(\theta_{k})\pi_{k}(\theta_{j})\right]} = \frac{1}{1+e^{-\Delta E_{jk}}},\tag{19}$$

where we recall the definition of  $\Delta E_{jk} := [U(\theta_j) - U(\theta_k)][1/T_j - 1/T_k]$ . It is obvious that  $\alpha_{jk}^B$  satisfies (18). Therefore, as long as we accept a swap with the energy difference  $\Delta E$  according to the probability  $\alpha_{jk}^B$ , detailed balance will definitely be preserved.

It should be obvious that equation (19) resembles the logistic function  $g(z) = 1/[1 + e^{-z}]$  in  $\Delta E_{jk}$ , which is exactly the cumulative distribution function of the standard logistic distribution  $\mathcal{L}(0, 1)$ . The acceptance test essentially checks whether the condition  $z_{\mathcal{L}} + \Delta E_{jk} > 0$  is met provided  $z_{\mathcal{L}} \sim \mathcal{L}(0, 1)$ , because the symmetric nature of  $\mathcal{L}(0, 1)$  guarantees  $\Pr[z_{\mathcal{L}} + \Delta E_{jk} > 0] = \Pr[z_{\mathcal{L}} \leq \Delta E_{jk}] = g(\Delta E_{jk})$ . However, problem arises when using mini-batches: the potential difference  $\Delta E_{jk}$  has been "corrupted" by Gaussian noise  $z_{\mathcal{N}}$ . We tackle this with the decomposition approach proposed by Seita *et al.* [34], where an auxiliary random variable  $z_{\mathcal{L}}$  is introduced to fix the Gaussian perturbation for an accurate logistic outcome. The new condition to be tested in the mini-batch setting can therefore be derived as  $z_{\mathcal{L}} + \Delta E_{jk} > 0 \iff z_{\mathcal{L}} + \Delta E_{jk} > 0 \iff z_{\mathcal{L}} + \Delta E_{jk} > 0 \iff z_{\mathcal{L}} + \Delta E_{jk} > 0$ . In other words, with mini-batching, one has to verify whether the sum of the correction variable  $z_{\mathcal{L}}$  and the estimate  $\Delta \tilde{E}_{jk}$  is positive for the decision of accepting a swapping attempt.

The objective now is to finding the correction distribution and then sampling  $z_{\mathscr{C}}$  from it, which relies on the solution to  $z_{\mathscr{C}}$ 's density function  $q_{\mathscr{C}}(z)$ . Instead of launching brutal-force attack with an arsenal of numerical solvers, we provide an analytic treatment that is more efficient and easier to reproduce. Requiring  $z_{\mathscr{L}} = z_{\mathscr{C}} + z_{\mathscr{N}}$  to hold for the three random variables, this condition unfortunately leads to a pathological correction distribution. Intuitively, the density  $q_{\mathscr{N}_{\sigma^2}}(z)$  of the Gaussian  $z_{\mathscr{N}}$  decays much faster than  $q_{\mathscr{L}}(z)$  of the logistic variable  $z_{\mathscr{L}}$  in the tails. Hence, the spectrum of  $q_{\mathscr{C}}(z)$  will not vanish at infinity; on the contrary,  $q_{\mathscr{C}}(z)$  must grow exponentially as z increases for perfect compensation.

Equation (6) defines a Gaussian deconvolution problem [20] w.r.t. the standard logistic distribution. Then we apply the Fourier transform to (6), which converts the convolution equation of densities into the corresponding algebraic equation of the associated characteristics functions:

$$\phi_{\mathcal{L}}(\omega) = \phi_{\mathcal{C}}(\omega) \cdot \phi_{\mathcal{N}_{\sigma^2}}(\omega), \text{ where } \phi_{\mathcal{L}}(\omega) = \frac{\pi \omega}{\sinh \pi \omega}, \phi_{\mathcal{N}_{\sigma^2}}(\omega) = \exp\left[-\frac{\sigma^2 \omega^2}{2}\right].$$
 (20)

From (20) it can be verified that  $\phi_{\mathscr{C}}(\omega)$  explodes as  $\omega \to \infty$ ; the associated  $q_{\mathscr{C}}(z)$  is thus ill-defined.

Fortunately, it is always possible for us to seek for an approximate solution to this ill-posed problem at an arbitrary level of precision. We introduce a specific kernel  $\psi_{\lambda}(\omega)$  with the bandwidth  $1/\lambda$  into the inverse Fourier transform of  $\phi_{\mathscr{C}}(\omega)$  as the decay factor [12]:

$$\hat{q}_{\mathscr{C}}(z) := \mathscr{F}^{-1} \left[ \psi_{\lambda}(\omega) \cdot \phi_{\mathscr{C}}(\omega) \right] = \frac{1}{2\pi} \int_{-\infty}^{\infty} \left[ \frac{\psi_{\lambda}(\omega)}{\phi_{\mathcal{N}_{\sigma^{2}}}(\omega)} \right] \phi_{\mathscr{L}}(\omega) e^{-iz\omega} d\omega, \tag{21}$$

where  $\psi_{\lambda}(\omega) := e^{-\lambda^2 \omega^4}$  serves as a "low-pass filter" selecting components within a limited bandwidth and suppressing high frequencies in the spectrum so that an approximate solution will be guaranteed. We would like to evaluate (21) using the series rather than direct integration. Consider the ratio inside the bracket in (21), it resembles the generating function of the Hermite polynomials  $H_n[u]$  (cf. [1]):

$$\frac{\psi_{\lambda}(\omega)}{\phi_{\mathcal{N}_{\sigma^2}}(\omega)} = \frac{e^{-\lambda^2 \omega^4}}{e^{-\sigma^2 \omega^2/2}} = \exp\left[2\left(\sigma^2/4\lambda\right) \cdot (\lambda\omega^2) - (\lambda\omega^2)^2\right] = \sum_{n=0}^{\infty} \frac{\lambda^n}{n!} H_n\left[\sigma^2/4\lambda\right] \cdot \omega^{2n}. \tag{22}$$

Now we substitute (22) back into (21) and rearrange the terms, which results in the series solution:

$$\hat{q}_{\mathscr{C}}(z) = \frac{1}{2\pi} \int_{-\infty}^{\infty} \left[ \sum_{n=0}^{\infty} \frac{\lambda^{n}}{n!} H_{n} \left[ \sigma^{2} / 4\lambda \right] \cdot \omega^{2n} \right] \phi_{\mathscr{L}}(\omega) e^{-iz\omega} d\omega$$

$$= \sum_{n=0}^{\infty} \left\{ \frac{\lambda^{n}}{n! i^{2n}} H_{n} \left[ \sigma^{2} / 4\lambda \right] \cdot \left[ \frac{1}{2\pi} \int_{-\infty}^{\infty} (i\omega)^{2n} \phi_{\mathscr{L}}(\omega) e^{-iz\omega} d\omega \right] \right\} = \sum_{n=0}^{\infty} \frac{(-\lambda)^{n}}{n!} H_{n} \left[ \sigma^{2} / 4\lambda \right] \cdot q_{\mathscr{L}}^{(2n)}(z), \quad (23)$$

where  $q_{\mathscr{L}}^{(2n)}(z) \coloneqq \frac{\mathrm{d}^{2n}}{\mathrm{d}z^{2n}} q_{\mathscr{L}}(z)$  denotes the 2n-th derivative of the logistic density and consequently the (2n+1)-th derivative of the logistic function g(z). We exploited the property of the Fourier transform regarding derivatives in the last equality of (23). Notice that as one formally sends  $\lambda \to 0_+$  the series approximation (23) becomes more and more accurate, and converges asymptotically as stated by (7), *i.e.* for any level of precision, we can always find a bandwidth  $\lambda$ , with which the analytical solution  $\hat{q}_{\mathscr{C}}$  approximates the real improper  $q_{\mathscr{C}}$ . With a sample from the approximation, we can practically approach a "quasi-balanced" condition.

#### D Proof of Theorem 3

*Proof.* We firstly recall equation (9). We define the integral in the last equity as the temperature-independent density of states, formulated as

$$N_j(E) := \int \delta[E - U(\theta_j)] \, \mathrm{d}\theta_j \tag{24}$$

such that the tempered energy distribution is re-written as

$$\tilde{\pi}_i^A(E) \propto N_i(E) e^{-\left[E + A_i(E)\right]/T_i}$$
.

As stated in [3], the equilibrium of biasing potential  $A_j^{\gamma}(U) \coloneqq A_j^{\gamma}(U, t \to \infty)$  can be formulated as

$$A_{j}^{\gamma}(E) = -\frac{(\gamma - 1)}{\gamma} \cdot \left[ -T_{j} \log \pi_{j}(E) \right] = -\frac{(\gamma - 1)}{\gamma} \cdot T_{j} \log \left[ N_{j}(E) e^{-E/T_{j}} \right]^{-1} + \text{const}$$

$$= -\frac{(\gamma - 1)}{\gamma} \cdot \left[ E - T_{j} \log N(E) \right] + \text{const} , \qquad (25)$$

After WTE has converged, the actual potential is essentially the superposition  $U(\theta_j) + A_j^{\gamma}(U(\theta_j))$  of the biasing potential and the original unbiased one. With (24) and (25), the energy distribution reads

$$\pi_j^A(E) \propto \int \delta \left[ E - U(\theta_j) \right] e^{-\left[ U(\theta_j) + A_j^{\gamma}(U(\theta_j)) \right] / T_j} d\theta_j = \left[ \int \delta \left[ E - U(\theta_j) \right] d\theta_j \right] \exp \left[ -\frac{E + A_j^{\gamma}(E)}{T_j} \right]$$

$$= N(E) \exp \left[ -\frac{E + (\gamma - 1)T_j \log N(E)}{\gamma T_j} \right] = \left[ N(E) e^{-E/T_j} \right]^{1/\gamma} = \left[ \pi_j(E) \right]^{1/\gamma},$$

which would give an approximately same average  $\langle E \rangle$  as in the canonical ensemble but with the fluctuation  $\mathbf{var}[E]$  amplified by a factor of  $\gamma$  [3].

**Remark.** An intuitive example can be obtained when the energy distribution is Gaussian, i.e.  $\pi_j(E) \propto e^{-(E-\langle E \rangle)^2/2T_j}$ , the well-tempered distribution is also Gaussian with the exactly same average but larger variance  $\pi_j^A(E) = \left[\pi_j(E)\right]^{1/\gamma} \propto e^{-(E-\langle E \rangle)^2/2\gamma T_j}$ .

#### E An algorithmic description of the plain RENHD without WTE

In this subsection, we provide an alternative algorithm in Algorithm 3 that we refer to as the *plain* RENHD, where the WTE is disabled.

## Algorithm 3 Replica-exchange Nosé-Hoover dynamics without well-tempered ensemble

```
1: function NHDYNAMICS(\{\theta_i\}, \{T_i\}, model, \mathcal{D}, |\mathcal{S}|_{\text{nhd}}, N, \epsilon, \mu, c)
                                                                                                                                          ▶ NHD length N; \epsilon, \mu, c in (13)
             for all \{j\} do
                                                                                                                                                    ▶ all j running in parallel
                   v_j \sim \mathcal{N}(0, T_j \epsilon)

s_j \leftarrow c/T_j

for n = \text{RANGE}(1, N) do
 3:
 4:
  5:
                          \mathcal{S} \leftarrow \text{NEXTBATCH}(\mathcal{D}, |\mathcal{S}|_{\text{nhd}})
 6:
                                                                                                                                                  ▶ fetching new mini-batch
                          \tilde{f}_j \leftarrow \text{model.BACKWARD}(\theta_j, \mathcal{S})
                                                                                                                                       ▶ evaluating mini-batch gradient
 7:
                          v_{j} \leftarrow v_{j} + \tilde{f}_{j}\epsilon - s_{j}v_{j} + \mathcal{N}(0, 2c\epsilon)

\theta_{j} \leftarrow \theta_{j} + v_{j}

s_{j} \leftarrow s_{j} + \mu[v_{j}^{\mathsf{T}}v_{j}/d - T_{j}\epsilon]
                                                                                                                                     ▶ additional Gaussian noise added
 8:
 9:
10:
11:
              return \{\theta_i\}
12: MAIN:
13: \{\theta_i\} \leftarrow \text{RANDN}()
                                                                                                                                                                      ▶ initialization
14: args \leftarrow (|\mathcal{S}|_{nhd}, N, \epsilon, \mu, c)
                                                                                                                                                           ▶ packing arguments
15: loop
              \{\theta_i\} \leftarrow \text{NHDYNAMICS}(\{\theta_i\}, \{T_i\}, \text{model}, \mathcal{D}, \text{args})
16:
              \{(j,k)\} \leftarrow \text{RAND}()
                                                                                                                                  ▶ sampling a set of replicas to swap
17:
              for all \{(j, k)\} do
18:
19:
                    REPLICAEXCHANGE(\theta_i, \theta_k, model, \mathfrak{D}, |\mathcal{S}|_{\text{re}}, \sigma_*^2, \hat{q}_{\mathscr{C}})
                                                                                                                                                             ▶ recall Algorithm 1
20:
              samples \leftarrow [samples, \theta_0]
                                                                                                                        \triangleright \theta_0 from replica 0 recover true posterior
```